

Observable CP-violation in charmed baryons decays with SU(3) symmetry analysis

Jin Sun^{2,*}, Ruilin Zhu^{1,†} and Zhi-Peng Xing^{1‡}¹*Department of Physics and Institute of Theoretical Physics,
Nanjing Normal University, Nanjing, Jiangsu 210023, China*²*Particle Theory and Cosmology Group, Center for Theoretical Physics of the Universe,
Institute for Basic Science (IBS), Daejeon 34126, Korea*

CP violation in baryon decays has recently garnered significant attention. Traditionally, CP violation in charmed baryon decays is predicted to be at the order of $O(10^{-4})$. Utilizing recent measurements from BESIII, Belle and Belle II experiments, we conduct a comprehensive global analysis to estimate the contribution of topological diagrams in these processes. Our study reveals that topological diagrams alone cannot fully account for the experimental data. By incorporating new effects that are not included in traditional topological diagrams and exploring the possible source of the new effect, our analysis reveals the potential for significant CP violation in $\Lambda_c^+ \rightarrow n\pi^+$ and $\Xi_c^+ \rightarrow \Xi^0 K^+$. This suggests a promising opportunity to observe CP violation for the first time in charmed baryon decays.

Introduction- CP violation (CPV) is one of the most important issues in particle physics [1–15], necessary to explain the baryon-antibaryon asymmetry of the universe. However, CP violation is only observed in meson decays, and no conclusive signal of CP violation in baryon decays has been observed in particle physics experiments. The current observations of CP violation are not sufficient to explain the matter asymmetry of the universe, making the search for new sources of CP violation important.

Over the past 20 years, with the increasing number of measurements by BESIII, Belle, Belle II, and LHCb collaborations [16–26], charmed baryons decays have attracted more attention from both the experimental and theoretical community [27–37], particularly on anti-triplet charmed baryon two-body decays. More precise experimental measurements will advance the search for CP violation hidden in baryon decays.

In the general theoretical analysis of CPV in Ref. [38], the direct CPV of two-body decay processes is proportional to the weak phase difference and strong phase difference: $A_{CP} \propto \sin(\phi_1 - \phi_2) \sin(\delta_1 - \delta_2)$. Here, δ_i is the strong phase and ϕ_i is the weak phase from the CKM matrix element. For the charmed baryon two-body decays, the effective Hamiltonian \mathcal{H}_{eff} is given as

$$\mathcal{H}_{eff} = \frac{G_F}{\sqrt{2}} \left(\sum_{i=1,2} C_i \lambda O_i - \sum_{j=3}^6 C_j \lambda_b O_j \right) + h.c., \quad (1)$$

where $O_{1,2}$ is the current-current operator and $O_{3\sim 6}$ is QCD penguin operator. $\lambda = V_{cq}^* V_{uq'}$ with $q, q' = d, s$ and $\lambda_b = V_{cb}^* V_{ub}$. The specific expressions of these operators refer to Ref. [39]. Due to the different weak phases induced by the current-current operator and the penguin operator, the weak phase difference required by

CPV is naturally generated. However, in previous studies [40], the penguin operator is usually ignored owing to $|V_{cb}^* V_{ub}| \sim 10^{-4} \ll |V_{cs}^* V_{ud}|$, so that CPV cannot be emerged.

To search for possible CPV in charmed baryon decays, we introduce SU(3) flavor symmetry in our work. The SU(3) flavor symmetry analysis, including the irreducible representation amplitude (IRA) and the topological diagrammatic approach (TDA), is one of the most powerful method in charmed baryon two-body decays. Previous studies show that SU(3) flavor symmetry in anti-triplet charmed baryon two-body decay is a good symmetry [41]. In 2024, the BESIII Collaboration measured the decay branching ratios of Λ_c^+ , and the Belle and Belle II Collaborations measured the decay branching ratios and asymmetry parameters of Ξ_c^0 for the first time [42–44] as

$$\begin{aligned} Br(\Lambda_c^+ \rightarrow p\pi^0) &= (0.0156_{-0.0058}^{+0.0072} \pm 0.002)\%, \\ Br(\Lambda_c^+ \rightarrow p\eta) &= (0.163 \pm 0.031 \pm 0.011)\%, \\ Br(\Lambda_c^+ \rightarrow pK_L) &= (1.67 \pm 0.06 \pm 0.04)\%, \\ Br(\Xi_c^0 \rightarrow \Xi^0\pi^0) &= (0.69 \pm 0.03 \pm 0.05 \pm 0.13)\%, \\ Br(\Xi_c^0 \rightarrow \Xi^0\eta) &= (0.16 \pm 0.02 \pm 0.02 \pm 0.03)\%, \\ Br(\Xi_c^0 \rightarrow \Xi^0\eta') &= (0.12 \pm 0.03 \pm 0.01 \pm 0.02)\%, \\ \alpha(\Xi_c^0 \rightarrow \Xi^0\pi^0) &= -0.90 \pm 0.15 \pm 0.23. \end{aligned} \quad (2)$$

Based on the new measurements, it is possible to determine all SU(3) IRA amplitudes and further understand the weak interactions of charmed particles, including possible CPV effects.

In our analysis, we provide a global fit to determine all the IRA amplitudes in Ref. [41]. With the help of the equivalence between IRA and TDA, we can not only test the correctness of the topological diagrams but also estimate the value of each diagram in TDA. As a result, we find that although the topological diagrams in TDA are basically consistent with our IRA numerical results, the topological diagram which only includes the $O_{1,2}$ operator cannot perfectly explain our IRA results. Without loss of generality, we can use a new diagram to express the conflicting parts of IRA and TDA and

* sunjin0810@ibs.re.kr

† rlzhu@njnu.edu.cn

‡ zpxing@nnu.edu.cn(corresponding author)

include them in our fit. To analyze the possible CPV introduced by the new diagram, we explored two possible source of the new diagram: SU(3) symmetry breaking and penguin operator and determine their contribution respectively. Our analysis shows that the new diagram may introduce a large CPV and it is promising to be observed in future experiments.

The global analysis of anti-triplet charmed baryon two-body decays with IRA- Using SU(3) flavor symmetry, the anti-triplet charmed baryon, light baryon octet, and light meson octet can be expressed by 3×3 matrices $T_{c\bar{3}}$, T_8 , and P , respectively [41]. The SU(3) invariant decay amplitudes for anti-triplet charmed baryon two-body decays are constructed as $a_{15} \times \epsilon_{imn}(T_{c\bar{3}})^{[mn]}(H_{15})_j^{\{ik\}}(\bar{T}_8)_k^j P_l^i$ and $a_6 \times (T_{c\bar{3}})^{[ik]}(H_{\bar{6}})_{\{ij\}}(\bar{T}_8)_k^j P_l^i$. Here the effective weak interaction Hamiltonian with IRA method is decomposed: $3 \otimes \bar{3} \otimes 3 = 3 \oplus \bar{3} \oplus \bar{6} \oplus 15$. The nonzero matrix are $H_{\bar{6}}$ and H_{15} , which are expressed in Ref. [41]. By enumerating all possible matrix combinations, nine independent amplitudes can be constructed as $\{a, b_6, c_6, d_6\}$ and $\{a', b_{15}, c_{15}, d_{15}, e_{15}\}$. Using these nine SU(3) amplitudes, all amplitudes of anti-triplet charmed baryon two-body decays can be expressed.

To correctly describe the phenomenological results of anti-triplet charmed baryon two-body decays, each SU(3) amplitude can be expressed by parity-violating form factors $f_{6,15}^{b,c,d}, f^{a(i)}$ and parity-conserving form factors $g_{6,15}^{b,c,d}, g^{a(i)}$ as defined in Ref. [41]. Subsequently, the branching ratios and polarization parameters α are expressed in Ref. [40].

By assuming real form factors for simplicity, we perform fits with updated data in Eq. 2 and the latest PDG [38] using the nonlinear least- χ^2 method [45]. Here, we disregard the BESIII result $\alpha(\Lambda_c^+ \rightarrow \Xi^0 K^+) = 0.01 \pm 0.16 \pm 0.03$ [46] because it has a large error compared to the central value and is inconsistent with our previous work [41]. In addition the channel $\Xi_c^0 \rightarrow \Xi^0 \pi^0$ contributes the most to the χ^2 while the channel $\Lambda_c^+ \rightarrow \Xi^0 K^+$ contributes less in the preliminary analysis. Therefore, we attempt to exclude this measurement from the global fit and obtain the fit results (Case I) in Table I.

However, we predict $\alpha(\Lambda_c \rightarrow \Sigma^0 K^+) = -0.9971 \pm 0.0036$ in this method, which deviates by 2σ from the experimental data $\alpha(\Lambda_c \rightarrow \Sigma^0 K^+)_{\text{exp}} = -0.54 \pm 0.20$. This indicates that the assumption of real form factors is inadequate, prompting us to further explore the complex case (Case II) in the following.

The comprehensive analysis of anti-triplet charmed baryon two-body decays with the equivalence of TDA and IRA- All nine IRA amplitudes and 18 form factors can be determined based on the key experimental results measured by Belle and Belle II, as shown in Table I. This facilitates an in-depth study

of anti-triplet charmed baryon two-body decays. A comprehensive analysis can be provided by introducing the topological diagrammatic approach (TDA), which offers more intuitive physical images. In fact, the two different methods (IRA and TDA) are mutually equivalent, as studied in Refs. [33, 47, 48]. In our work, we use the same notation for TDA amplitudes $\bar{a}_{1\sim 19}$ in Ref. [33]. The corresponding topological diagrams are shown in Fig. 1.

Using the definition $(T_8)_{ijk} = \epsilon_{ijl}(\bar{T}_8)_k^l$, the H_k^{ij} in TDA can be decomposed into IRA forms as $H_k^{ij} = \frac{1}{2} \left[(H_{15})^{ij} + \frac{1}{2} \epsilon^{ijl} (H_{\bar{6}})_{kl} \right]$. The transformation from TDA to IRA occurs naturally with the following relations for the parameters:

$$\begin{aligned} \bar{a}_1 &= b_6 - d_6 + e_{15}, & \bar{a}_2 &= d_6 - b_6 + e_{15}, & \bar{a}_3 &= -\frac{a}{2}, \\ \bar{a}_4 &= \frac{1}{2}(-c_6 + c_{15}), & \bar{a}_5 &= \frac{1}{2}a', & \bar{a}_7 &= \frac{1}{2}(c_6 + c_{15}), \\ \bar{a}_6 &= \frac{1}{2}(-b_6 - c_6 - e_{15} + d_{15}) + \frac{1}{4}(a + a'), \\ \bar{a}_8 &= \frac{1}{2}(b_6 + c_6 + d_{15} - e_{15}) - \frac{1}{4}(a + a'), \\ \bar{a}_9 &= \frac{1}{2}(a + a'), & \bar{a}_{12} &= c_6, & \bar{a}_{15} &= \frac{1}{2}(b_6 - d_6 + e_{15}), \\ \bar{a}_{10} &= \frac{1}{2}(-b_6 - c_{15} + d_{15} - e_{15}) + \frac{1}{4}(a + a'), \\ \bar{a}_{11} &= \frac{1}{2}(b_6 - c_{15} + d_{15} - e_{15}) - \frac{1}{4}(a + a'), \\ \bar{a}_{13} &= \frac{1}{2}(-e_{15} + b_{15} + c_6 + d_{15}) - \frac{1}{4}(a' - a) \\ \bar{a}_{14} &= \frac{1}{2}(-e_{15} + b_{15} - c_6 + d_{15}) - \frac{1}{4}(a' - a) \\ \bar{a}_{16} &= \frac{1}{2}(-b_6 + d_6 + e_{15}), & \bar{a}_{17} &= \frac{1}{2}(d_6 + e_{15} - b_{15}), \\ \bar{a}_{18} &= \frac{1}{2}(-d_6 + e_{15} - b_{15}), & \bar{a}_{19} &= d_6. \end{aligned} \quad (3)$$

By using the definition $\bar{a}_i = G_F \bar{u}(f_i - g_i \gamma_5)u$ with $i = 1 \sim 19$, the numerical results of the form factors for TDA are obtained in the lower panel of Table I.

Note that the diagrams $T_1 - T_2$ and $T_4 - T_5$ have the same topological structures, where one selects $\mathcal{M}_{T_1} = \mathcal{M}_{T_2}$ and $\mathcal{M}_{T_4} = \mathcal{M}_{T_5}$. The number of independent topological diagrams is reduced from seven to five, consistent with the latest TDA analysis in Ref. [48]. As demonstrated in Ref. [33], each topological diagram in Fig. 1 corresponds to more than one TDA amplitude. Therefore, it is assumed that the absolute value of the TDA amplitude with the same topological diagram should be equal. By defining the form factor $\mathcal{M}_{T_i} = G_F \bar{u}(f_{T_i} - g_{T_i} \gamma_5)u$, $i = 1 \sim 7$, one obtains the relations as

$$\begin{aligned} |A_{1,15}| &= A_{T_1} = |A_{2,16}| = A_{T_2}, & |A_{3,5,9}| &= A_{T_3}, \\ |A_{4,6,10}| &= A_{T_4} = |A_{7,8,11}| = A_{T_5}, \\ |A_{12,13,14}| &= A_{T_6}, & |A_{17,18,19}| &= A_{T_7}, \quad A = f, g. \end{aligned} \quad (4)$$

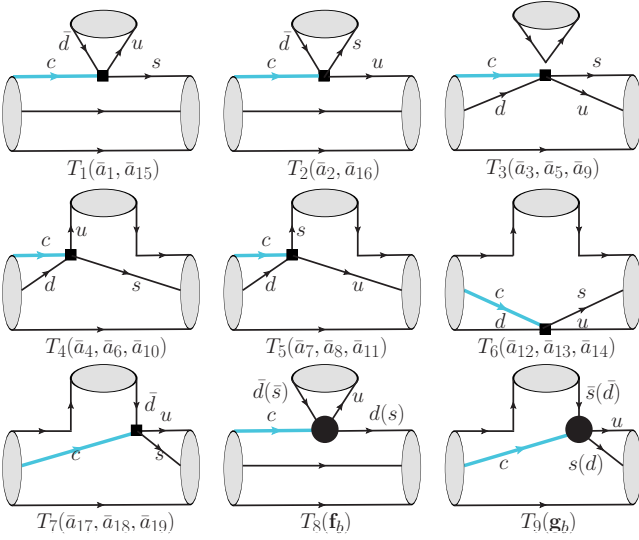


FIG. 1: Topology diagrams for the charmed baryon decays into an octet baryon and a light meson. Here T_{1-7} show the Cabibbo-favored channels $c \rightarrow u\bar{d}s$. $T_{8,9}$ describe the new effects in the Cabibbo-suppressed $c \rightarrow u\bar{d}(\bar{s}s)$ induced by \mathbf{f}_b and \mathbf{g}_b respectively.

The assumptions are approximately supported by the numerical results within 1σ in Table. I and it shows the diagram $T_{1,2}$ actually give the main contribution. However, some form factors contradict the assumption, such as $|f_{1,15}| - |f_{2,16}| \sim 0.06$, $|f_{T_{17,18}}| - |f_{19}| \sim 0.02$ and $|g_{17,19}| - |g_{18}| \sim 0.05$. To focus on the largest effects, we ignore the discrepancy involving f_{19} and primarily consider $|f_{1,15}| > |f_{2,16}|$ and $|g_{17,19}| > |g_{18}|$ in the subsequent analysis. This implies that there are other effects in the topology diagrams. For exploring the possible new effects, one defines the form factors \mathbf{f}_b and \mathbf{g}_b to absorb these effect as $\mathbf{f}_b = f_{T_1} - f_{T_2}$ and $\mathbf{g}_b = -g_{18} - g_{T_7}$. The corresponding topology diagrams $T_{8,9}$ are given in Fig. 1. Then the IRA form factors are expressed by TDA form factors and $\mathbf{f}_b, \mathbf{g}_b$ as

$$\begin{aligned}
 f^a &= -\frac{f_{T_6}}{2}, & f^{a'} &= \frac{1}{2}f_{T_6} - f_{T_3}, & f_6^b &= \frac{3}{2}\mathbf{f}_b, \\
 f_{15}^b &= -f_{T_6} - f_{T_7}, & f_6^c &= f_{T_6} + f_{T_4}, & f_{15}^c &= f_{T_4}, \\
 f_6^d &= -\frac{3}{2}\mathbf{f}_b - f_{T_7}, & f_{15}^d &= -2f_{T_4} - f_{T_6}, \\
 f_{15}^e &= -\frac{3}{2}\mathbf{f}_b + 3f_{T_1} + 2f_{T_4} + f_{T_6} + f_{T_7}, \\
 g^a &= g_{T_4} + \frac{g_{T_6}}{2}, & g^{a'} &= g_{T_4} + g_{T_3} - \frac{g_{T_6}}{2}, & g_{15}^c &= 0 \\
 g_6^b &= -3g_{T_1} - 2g_{T_4}, & g_{15}^b &= -g_{15}^e = \frac{\mathbf{g}_b}{2} + g_{T_6} + g_{T_7}, \\
 g_6^c &= g_{T_6}, & g_6^d &= 3g_{T_1} - g_{T_7} + \frac{\mathbf{g}_b}{2}, & g_{15}^d &= g_{T_6}. \quad (5)
 \end{aligned}$$

Since all the diagrams induced by $O_{1,2}$ are included in TDA diagrams T_{1-7} , it is reasonable to believe the diagrams $T_{8,9}$ are induced by SU(3) symmetry breaking or other operators like the penguin operators O_{3-6} . In

Eq. 5, we find that $g_{15}^c = 0$, which is consistent with our global fit (Case I) in Table. I. One can also directly observe that f_6^b depends only on new effect form factors, which provides us an ideal condition to study the contribution from new effects.

The strong phase in charmed baryon two-body decays and CPV- Recently, numerous SU(3) analyses have introduced a strong phase in the form factors to resolve the puzzle of the BESIII measurement $\alpha(\Lambda_c^+ \rightarrow \Xi^0 K^+) = 0.01 \pm 0.16 \pm 0.03$ [46]. In this section, we also analyze the situation using complex form factors (Case II) to conduct a comprehensive global analysis that incorporates all experimental data, including $\alpha(\Lambda_c^+ \rightarrow \Xi^0 K^+) = 0.01 \pm 0.16 \pm 0.03$ and $Br(\Xi_c^0 \rightarrow \Xi_0 \pi^0) = (0.69 \pm 0.03 \pm 0.05 \pm 0.13)\%$.

The above analysis demonstrates that the fits using the IRA method are largely consistent with the TDA assumption. Subsequently, we determine the strong phase from the perspective of topological diagrams. Since the strong phase arises from potential contributions of intermediate on-shell states in the decay process [38], the imaginary part of the form factor in Eq. 4 corresponding to each topological diagram is incorporated into our global analysis. Thus, the imaginary part of the IRA form factor in our fitting is derived using Eq. 5 under the assumption: $\mathcal{I}m(\mathbf{g}_b) = 0$. Additionally, we assume $\mathcal{I}m(f_{T_3}) = 0$ due to the global phase.

According to Eq.5, the IRA form factor f_6^b depends solely on the new effect, potentially leads to significant CP violation. To study the CPV, the possible sources of the new form factor \mathbf{f}_b are discussed. Since the form factor arises from the difference between topological diagrams T_1 and T_2 in Fig.1, the most likely source is the SU(3) symmetry breaking effect. Especially when long-distance interactions enter the interaction vertex in Fig.1, the flavor symmetry breaking effect must be involved. Additionally, the penguin operator in Eq. 1 can also contribute to the new form factor \mathbf{f}_b . When only flavor symmetry is considered, the difference in the Lorentz structure at the Hamiltonian vertex can be neglected. Consequently, the penguin operator has the same Hamiltonian matrix structure with the $O_{1,2}$ in TDA. However, in IRA, the penguin operator only contributes to H_3 , which is neglected in our work. Therefore, the new form factor \mathbf{f}_b introduced by the conflicting parts of IRA and TDA must be considered.

According to the above analysis, the form factor can be divided into two parts $\mathbf{f}_b = \mathbf{f}_b^S + \mathbf{f}_b^P e^{i\phi^P}$, where \mathbf{f}_b^S comes from the SU(3) symmetry breaking and $\mathbf{f}_b^P e^{i\phi^P}$ represents the penguin operator contribution with its weak phase $\phi^P = -1.147 \pm 0.026$. Including the two part of \mathbf{f}_b , the

TABLE I: The fit results for the real (Case I), complex (Case II) and TDA form factors.

form factors	Case I ($\chi^2/d.o.f=1.28$)				
vector(f)	$f^a = 0.0101(28)$	$f_6^b = 0.0187(40)$	$f_6^c = 0.0237(36)$	$f_6^d = -0.0093(37)$	$f^{a'} = -0.003(101)$
	$f_{15}^b = -0.0100(34)$	$f_{15}^c = 0.0073(34)$	$f_{15}^d = -0.0156(22)$	$f_{15}^e = 0.0537(35)$	
axial-vector(g)	$g^a = -0.0266(78)$	$g_6^b = -0.1784(55)$	$g_6^c = 0.0878(91)$	$g_6^d = -0.0556(72)$	$g^{a'} = 0.05(44)$
	$g_{15}^b = 0.0746(48)$	$g_{15}^c = 0.0075(90)$	$g_{15}^d = -0.0219(57)$	$g_{15}^e = 0.0189(34)$	
form factors	Case II ($\chi^2/d.o.f=0.875$)				
	real part			imaginary part	
vector(f)	$f^a = 0.0353(67)$	$f_6^c = -0.016(14)$	$f_6^d = -0.009(15)$	$f_{T_1} = 0.009(14)$	$f_{T_4} = -0.005(16)$
	$f^{a'} = -0.006(32)$	$\mathcal{R}e(\mathbf{f}_b^S) = -0.007(14)$	$\mathcal{R}e(\mathbf{f}_b^P) = 0.00060(20)$	$\mathcal{I}m(\mathbf{f}_b^S) = 0.003(16)$	$\mathcal{I}m(\mathbf{f}_b^P) = 0.0013(18)$
	$f_{15}^b = -0.021(12)$	$f_{15}^c = 0.0047(52)$	$f_{15}^d = 0.015(16)$	$f_{T_6} = 0.020(21)$	$f_{T_7} = -0.012(33)$
	$f_{15}^e = 0.012(12)$				
axial-vector(g)	$g^a = 0.003(29)$	$g_6^b = -0.035(18)$	$g_6^c = 0.034(37)$	$g_{T_1} = 0.019(34)$	$g_{T_3} = 0.13(76)$
	$g_6^d = -0.041(71)$	$g^{a'} = -0.06(50)$		$g_{T_4} = -0.104(84)$	$g_{T_6} = -0.026(51)$
	$g_{15}^b = 0.188(59)$	$g_{15}^c = 0.022(41)$	$g_{15}^d = 0.013(51)$	$g_{T_7} = -0.014(71)$	
	$g_{15}^e = 0.006(53)$				
form factors	TDA				
vector(f)	T_1	T_2	T_3	T_4	T_5
	$f_1 = 0.0817(45)$	$f_2 = 0.0257(50)$	$f_3 = -0.0051(14)$	$f_4 = -0.0082(12)$	$f_7 = 0.0155(33)$
	$f_{15} = 0.0409(23)$	$f_{16} = 0.0129(25)$	$f_5 = -0.002(50)$	$f_6 = -0.054(26)$	$f_8 = -0.015(25)$
			$f_9 = 0.003(50)$	$f_{10} = -0.046(26)$	$f_{11} = -0.031(24)$
	T_6	T_7			
	$f_{12} = 0.0237(36)$	$f_{17} = 0.0272(18)$			
	$f_{13} = -0.024(25)$	$f_{18} = 0.0365(35)$			
$f_{14} = -0.048(24)$	$f_{19} = -0.0093(37)$				
axial-vector(g)	T_1	T_2	T_3	T_4	T_5
	$g_1 = -0.1039(86)$	$g_2 = 0.1416(77)$	$g_3 = 0.0133(39)$	$g_4 = -0.0401(30)$	$g_7 = 0.0477(86)$
	$g_{15} = -0.0519(43)$	$g_{16} = 0.0708(38)$	$g_5 = 0.03(22)$	$g_6 = 0.03(11)$	$g_8 = -0.07(11)$
			$g_9 = 0.01(22)$	$g_{10} = 0.07(11)$	$g_{11} = -0.12(11)$
	T_6	T_7			
	$g_{12} = 0.0878(91)$	$g_{17} = -0.0557(37)$			
	$g_{13} = 0.04(11)$	$g_{18} = -0.00004(564)$			
$g_{14} = -0.05(11)$	$g_{19} = -0.0556(72)$				

form factors in our global analysis are defined as

$$\begin{aligned}
A_{6,15}^q &= e^{i\phi_1} \left(\mathcal{R}e(A_{6,15}^q) + \mathcal{I}m(A_{6,15}^q) \right), \\
f_6^b &= \frac{3}{2} \left(e^{i\phi_1} \left(\mathcal{R}e(\mathbf{f}_b^S) + \mathcal{I}m(\mathbf{f}_b^S) \right) \right. \\
&\quad \left. + e^{i\phi^P} \left(\mathcal{R}e(\mathbf{f}_b^P) + \mathcal{I}m(\mathbf{f}_b^P) \right) \right), \\
f_6^d &= e^{i\phi_1} \left(\mathcal{R}e(f_6^d) + \mathcal{I}m(f_6^d) \right) \\
&\quad - e^{i\phi^P} \frac{3}{2} \left(\mathcal{R}e(\mathbf{f}_b^P) + \mathcal{I}m(\mathbf{f}_b^P) \right), \\
f_{15}^e &= e^{i\phi_1} \left(\mathcal{R}e(f_{15}^e) + \mathcal{I}m(f_{15}^e) \right) \\
&\quad - e^{i\phi^P} \frac{3}{2} \left(\mathcal{R}e(\mathbf{f}_b^P) + \mathcal{I}m(\mathbf{f}_b^P) \right), \quad A = f, g, \quad (6)
\end{aligned}$$

where $q = a, b, c, d, e$. The weak phase ϕ_1 arises from the current-current operator as $\phi_1 = \arg(V_{cq}^* V_{uq'}) \approx 0, -\pi$.

One can find that the penguin operator only contributes to the Cabibbo-suppressed processes. The SU(3) symmetry requires the form factor corresponding to different processes to be equal [48, 49], one has the chance to determine the form factor \mathbf{f}_b^S by the Cabibbo-allowed and doubly Cabibbo-suppressed processes. Based on the symmetry breaking form factor we derived, the penguin contribution form factor \mathbf{f}_b^P can be further determined by the Cabibbo-suppressed processes.

By introducing the weak phase of penguin operator ϕ^T , one can derive the CPV if the global fit gives a nonzero value of \mathbf{f}_b^P . In our analysis, we obtain the fit results with $\chi^2/d.o.f = 0.875$, indicating that our fit is reasonable and the form factors effectively explain the experimental data.

With the determined penguin operator contribution $\mathcal{R}e(\mathbf{f}_b^P) = 0.0006(2)$ and $\mathcal{I}m(\mathbf{f}_b^P) = 0.0013(18)$, one

can predict the CP violation (A_{CP}) for the Cabibbo-suppressed processes. Considering the ratio of the form factor from current-current and penguin operator $\frac{\langle O_{1,2} \rangle}{\langle O_{3-6} \rangle} \sim O(10^{-2})$, our study implies that the contribution of the QCD penguin may be more substantial than conventionally assumed, necessitating further theoretical investigation in the future.

Based on the fitted results, we predict the values A_{CP} for the Cabibbo-suppressed processes and found that almost all the predicted A_{CP} values are approximately zero within errors, except for the following processes

$$A_{CP}^{\Lambda_c^+ \rightarrow n\pi^+} = 0.076(57), A_{CP}^{\Xi_c^+ \rightarrow \Xi^0 K^+} = 0.092(70). \quad (7)$$

We strongly recommend the experimental measurement of the processes: $\Lambda_c^+ \rightarrow n\pi^+$ since their branching ratio has been measured.

Conclusion- In our study, we investigate the equivalence of the SU(3) IRA and TDA methods through a global analysis (case I). Our findings indicate that the results obtained from the IRA method align well with the assumptions made in TDA, as illustrated by the topological diagram in Fig. 1. Nonetheless, certain form factors show discrepancies compared to the predicted values from the topological diagrams. To assess the extent of these discrepancies, we employ the form factors \mathbf{f}_b and \mathbf{g}_b to characterize the new effects.

By leveraging the equivalence between IRA and TDA

methods, our global analysis extends to complex form factors. By considering the SU(3) symmetry breaking and penguin operator as the source of form factor \mathbf{f}_b , the corresponding contributions of SU(3) symmetry breaking and penguin operator are determined through global analysis respectively. Then we further explore CP violation in anti-triplet charmed baryon two-body decay processes. Our analysis yields non-zero A_{CP} in Eq. 7. Considering its error, the observable CP violation can be observed at the order of $O(10^{-2})$. We strongly advocate for measuring these processes.

Note that the most ideal condition for measuring CPV is to produce charmed baryon and anti-baryon pairs simultaneously. The BESIII Collaborations meet these conditions due to the most data on $\Lambda_c \bar{\Lambda}_c$ and $\Xi_c \bar{\Xi}_c$ pairs. For $\Lambda_c^+ \rightarrow n\pi^+$, their branching ratio has been measured by the BESIII Collaborations. Therefore, it holds the potential for observing CP violation in charmed baryon decays at this experimental facilities for the first time.

ACKNOWLEDGMENTS

We thank Prof. Xiao-Gang He, Prof. Wei Wang and Prof. YuJi Shi for useful discussion. The work of Jin Sun is supported by IBS under the project code, IBS-R018-D1. The work of Ruilin Zhu is supported by NSFC under grant No. 12322503 and No. 12075124, and by Natural Science Foundation of Jiangsu under Grant No. BK20211267. The work of Zhi-Peng Xing is supported by NSFC under grant No.12375088 and No. 12335003.

-
- [1] T. D. Lee and C.-N. Yang, “General Partial Wave Analysis of the Decay of a Hyperon of Spin 1/2,” *Phys. Rev.* **108** (1957) 1645–1647.
- [2] M. Kobayashi and T. Maskawa, “CP Violation in the Renormalizable Theory of Weak Interaction,” *Prog. Theor. Phys.* **49** (1973) 652–657.
- [3] N. G. Deshpande and X.-G. He, “CP asymmetry relations between anti-b0 \rightarrow pi pi and anti-b0 \rightarrow pi K rates,” *Phys. Rev. Lett.* **75** (1995) 1703–1706, [arXiv:hep-ph/9412393](#).
- [4] **LHCb** Collaboration, R. Aaij *et al.*, “Observation of CP Violation in Charm Decays,” *Phys. Rev. Lett.* **122** no. 21, (2019) 211803, [arXiv:1903.08726 \[hep-ex\]](#).
- [5] A. Lenz and G. Wilkinson, “Mixing and CP Violation in the Charm System,” *Ann. Rev. Nucl. Part. Sci.* **71** (2021) 59–85, [arXiv:2011.04443 \[hep-ph\]](#).
- [6] S. Schacht and A. Soni, “Enhancement of charm CP violation due to nearby resonances,” *Phys. Lett. B* **825** (2022) 136855, [arXiv:2110.07619 \[hep-ph\]](#).
- [7] I. Bediaga, T. Frederico, and P. C. Magalhães, “Enhanced Charm CP Asymmetries from Final State Interactions,” *Phys. Rev. Lett.* **131** no. 5, (2023) 051802, [arXiv:2203.04056 \[hep-ph\]](#).
- [8] J.-P. Wang and F.-S. Yu, “Probing hyperon CP violation with charmed baryon decays,” *Phys. Lett. B* **849** (2024) 138460, [arXiv:2208.01589 \[hep-ph\]](#).
- [9] J.-P. Wang, Q. Qin, and F.-S. Yu, “CP violation induced by T-odd correlations and its baryonic application,” [arXiv:2211.07332 \[hep-ph\]](#).
- [10] **LHCb** Collaboration, S. Maccolini, “Mixing and CPV in charm decays at LHCb,” *PoS FPCP2023* (2023) 081.
- [11] Y.-F. Shen, J.-P. Wang, and Q. Qin, “Possible large CP violation in charmed Λ_b decays,” *Phys. Rev. D* **108** no. 11, (2023) L111901, [arXiv:2309.09854 \[hep-ph\]](#).
- [12] W.-J. Song, Y.-F. Shen, and Q. Qin, “Double-mixing CP violation in B decays,” [arXiv:2403.01904 \[hep-ph\]](#).
- [13] X.-G. He and C.-W. Liu, “Large CP violation in charmed baryon decays,” [arXiv:2404.19166 \[hep-ph\]](#).
- [14] S. Schacht, “Charm CP violation and searches,” in *58th Rencontres de Moriond on Electroweak Interactions and Unified Theories*. 5, 2024. [arXiv:2405.09299 \[hep-ph\]](#).
- [15] D. Wang and J.-F. Luo, “Topological diagrams of

- charmed baryon decays in the $SU(3)_F$ limit,”
arXiv:2406.14061 [hep-ph].
- [16] Belle Collaboration, R. Mizuk *et al.*, “Observation of an isotriplet of excited charmed baryons decaying to Lambda+(c) pi,” *Phys. Rev. Lett.* **94** (2005) 122002, arXiv:hep-ex/0412069.
- [17] Belle Collaboration, G. Pakhlova *et al.*, “Observation of a near-threshold enhancement in the $e^+e^- \rightarrow$ Lambda+(c) Lambda-(c) cross section using initial-state radiation,” *Phys. Rev. Lett.* **101** (2008) 172001, arXiv:0807.4458 [hep-ex].
- [18] LHCb Collaboration, R. Aaij *et al.*, “Prompt charm production in pp collisions at sqrt(s)=7 TeV,” *Nucl. Phys. B* **871** (2013) 1–20, arXiv:1302.2864 [hep-ex].
- [19] LHCb Collaboration, R. Aaij *et al.*, “Differential branching fraction and angular analysis of $\Lambda_b^0 \rightarrow \Lambda \mu^+ \mu^-$ decays,” *JHEP* **06** (2015) 115, arXiv:1503.07138 [hep-ex]. [Erratum: JHEP 09, 145 (2018)].
- [20] BESIII Collaboration, M. Ablikim *et al.*, “Measurement of the absolute branching fraction for $\Lambda_c^+ \rightarrow \Lambda e^+ \nu_e$,” *Phys. Rev. Lett.* **115** no. 22, (2015) 221805, arXiv:1510.02610 [hep-ex].
- [21] BESIII Collaboration, M. Ablikim *et al.*, “Measurements of absolute hadronic branching fractions of Λ_c^+ baryon,” *Phys. Rev. Lett.* **116** no. 5, (2016) 052001, arXiv:1511.08380 [hep-ex].
- [22] LHCb Collaboration, R. Aaij *et al.*, “Observation of five new narrow Ω_c^0 states decaying to $\Xi_c^+ K^-$,” *Phys. Rev. Lett.* **118** no. 18, (2017) 182001, arXiv:1703.04639 [hep-ex].
- [23] BESIII Collaboration, M. Ablikim *et al.*, “Precision measurement of the $e^+e^- \rightarrow \Lambda_c^+ \bar{\Lambda}_c^-$ cross section near threshold,” *Phys. Rev. Lett.* **120** no. 13, (2018) 132001, arXiv:1710.00150 [hep-ex].
- [24] Belle Collaboration, J. Yelton *et al.*, “Observation of Excited Ω_c Charmed Baryons in e^+e^- Collisions,” *Phys. Rev. D* **97** no. 5, (2018) 051102, arXiv:1711.07927 [hep-ex].
- [25] LHCb Collaboration, R. Aaij *et al.*, “First Observation of the Doubly Charmed Baryon Decay $\Xi_{cc}^{++} \rightarrow \Xi_c^+ \pi^+$,” *Phys. Rev. Lett.* **121** no. 16, (2018) 162002, arXiv:1807.01919 [hep-ex].
- [26] LHCb Collaboration, R. Aaij *et al.*, “Measurement of the Ω_c^0 baryon lifetime,” *Phys. Rev. Lett.* **121** no. 9, (2018) 092003, arXiv:1807.02024 [hep-ex].
- [27] W. Roberts and M. Pervin, “Heavy baryons in a quark model,” *Int. J. Mod. Phys. A* **23** (2008) 2817–2860, arXiv:0711.2492 [nucl-th].
- [28] R. A. Briceno, H.-W. Lin, and D. R. Bolton, “Charmed-Baryon Spectroscopy from Lattice QCD with $N_f = 2+1+1$ Flavors,” *Phys. Rev. D* **86** (2012) 094504, arXiv:1207.3536 [hep-lat].
- [29] O. Romanets, L. Tolos, C. Garcia-Recio, J. Nieves, L. L. Salcedo, and R. G. E. Timmermans, “Charmed and strange baryon resonances with heavy-quark spin symmetry,” *Phys. Rev. D* **85** (2012) 114032, arXiv:1202.2239 [hep-ph].
- [30] Z. S. Brown, W. Detmold, S. Meinel, and K. Orginos, “Charmed bottom baryon spectroscopy from lattice QCD,” *Phys. Rev. D* **90** no. 9, (2014) 094507, arXiv:1409.0497 [hep-lat].
- [31] C.-D. Lü, W. Wang, and F.-S. Yu, “Test flavor SU(3) symmetry in exclusive Λ_c decays,” *Phys. Rev. D* **93** no. 5, (2016) 056008, arXiv:1601.04241 [hep-ph].
- [32] X.-G. He and W. Wang, “Flavor SU(3) Topological Diagram and Irreducible Representation Amplitudes for Heavy Meson Charmless Hadronic Decays: Mismatch and Equivalence,” *Chin. Phys. C* **42** no. 10, (2018) 103108, arXiv:1803.04227 [hep-ph].
- [33] X.-G. He, Y.-J. Shi, and W. Wang, “Unification of Flavor SU(3) Analyses of Heavy Hadron Weak Decays,” *Eur. Phys. J. C* **80** no. 5, (2020) 359, arXiv:1811.03480 [hep-ph].
- [34] H. J. Zhao, Y.-L. Wang, Y. K. Hsiao, and Y. Yu, “A diagrammatic analysis of two-body charmed baryon decays with flavor symmetry,” *JHEP* **02** (2020) 165, arXiv:1811.07265 [hep-ph].
- [35] M. He and R. Rapp, “Charm-Baryon Production in Proton-Proton Collisions,” *Phys. Lett. B* **795** (2019) 117–121, arXiv:1902.08889 [nucl-th].
- [36] C. Q. Geng, C.-W. Liu, and T.-H. Tsai, “Asymmetries of anti-triplet charmed baryon decays,” *Phys. Lett. B* **794** (2019) 19–28, arXiv:1902.06189 [hep-ph].
- [37] C.-P. Jia, D. Wang, and F.-S. Yu, “Charmed baryon decays in $SU(3)_F$ symmetry,” *Nucl. Phys. B* **956** (2020) 115048, arXiv:1910.00876 [hep-ph].
- [38] Particle Data Group Collaboration, S. N. *et al.*, “Review of Particle Physics,” *to be published in Phys. Rev. D* **110** (2024) 030001.
- [39] G. Buchalla, A. J. Buras, and M. E. Lautenbacher, “Weak decays beyond leading logarithms,” *Rev. Mod. Phys.* **68** (1996) 1125–1144, arXiv:hep-ph/9512380.
- [40] M. He, X.-G. He, and G.-N. Li, “CP-Violating Polarization Asymmetry in Charmless Two-Body Decays of Beauty Baryons,” *Phys. Rev. D* **92** no. 3, (2015) 036010, arXiv:1507.07990 [hep-ph].
- [41] Z.-P. Xing, X.-G. He, F. Huang, and C. Yang, “Global analysis of measured and unmeasured hadronic two-body weak decays of antitriplet charmed baryons,” *Phys. Rev. D* **108** no. 5, (2023) 053004.
- [42] BESIII Collaboration, M. Ablikim *et al.*, “Evidence of the singly Cabibbo suppressed decay $\Lambda_c^+ \rightarrow p \pi^0$,” *Phys. Rev. D* **109** no. 9, (2024) L091101, arXiv:2311.06883 [hep-ex].
- [43] Belle-II, Belle Collaboration, I. Adachi *et al.*, “Measurements of the branching fractions of $\Xi_c^0 \rightarrow \Xi^0 \pi^0$, $\Xi_c^0 \rightarrow \Xi^0 \eta$, and $\Xi_c^0 \rightarrow \Xi^0 \eta'$ and asymmetry parameter of $\Xi_c^0 \rightarrow \Xi^0 \pi^0$,” arXiv:2406.04642 [hep-ex].
- [44] BESIII Collaboration, M. Ablikim *et al.*, “Measurements of K_S^0 - K_L^0 asymmetries in the decays $\Lambda_c^+ \rightarrow p K_{L,S}^0$, $p K_{L,S}^0 \pi^+ \pi^-$ and $p K_{L,S}^0 \pi^0$,” arXiv:2406.18083 [hep-ex].
- [45] P. Lepage and C. Gohlke, “gplepage/lqfit: lqfit version 13.2.2(v13.2),zenodo doi.org/10.5281/zenodo.4037174.”
- [46] BESIII Collaboration, M. Ablikim *et al.*, “First

- Measurement of the Decay Asymmetry in the Pure
W-Boson-Exchange Decay $\Lambda_c^+ \rightarrow \Xi^0 K^+$,”
Phys. Rev. Lett. **132** no. 3, (2024) 031801,
[arXiv:2309.02774 \[hep-ex\]](#).
- [47] Y. K. Hsiao, Y. L. Wang, and H. J. Zhao, “Equivalent
 $SU(3)_f$ approaches for two-body anti-triplet charmed
baryon decays,” *JHEP* **09** (2022) 035,
[arXiv:2111.04124 \[hep-ph\]](#).
- [48] H. Zhong, F. Xu, and H.-Y. Cheng, “Analysis of
hadronic weak decays of charmed baryons in the
topological diagrammatic approach,”
Phys. Rev. D **109** no. 11, (2024) 114027,
[arXiv:2404.01350 \[hep-ph\]](#).
- [49] C.-Q. Geng, X.-G. He, X.-N. Jin, C.-W. Liu, and
C. Yang, “Complete determination of $SU(3)_F$
amplitudes and strong phase in $\Lambda_c^+ \rightarrow \Xi^0 K^+$,”
Phys. Rev. D **109** no. 7, (2024) L071302,
[arXiv:2310.05491 \[hep-ph\]](#).

Supplemental Material

TABLE II: Experimental data and fitting results of anti-triplet charmed baryons two-body decays for two different fits. Case I(II) means the fit results for the real(complex) form factors.

channel	exp		Case I		Case II	
	Br(%)	α	Br(%)	α	Br(%)	α
$\Lambda_c^+ \rightarrow p\pi^0$	0.0156(75)		0.0174(53)		0.0160(71)	
$\Lambda_c^+ \rightarrow pK_S^0$	1.59(7)	0.2(5)	1.646(48)	0.41(12)	1.590(56)	0.05(27)
$\Lambda_c^+ \rightarrow pK_L^0$	1.67(7)		1.646(48)		1.685(60)	
$\Lambda_c^+ \rightarrow p\eta$	0.158(11)		0.158(11)		0.154(11)	
$\Lambda_c^+ \rightarrow p\eta'$	0.0484(91)		0.0464(61)		0.0513(75)	
$\Lambda_c^+ \rightarrow \Lambda\pi^+$	1.29(5)	-0.755(6)	1.305(47)	-0.7538(60)	1.292(48)	-0.7551(60)
$\Lambda_c^+ \rightarrow \Sigma^0\pi^+$	1.27(6)	-0.466(18)	1.259(46)	-0.471(15)	1.259(49)	-0.472(15)
$\Lambda_c^+ \rightarrow \Sigma^+\pi^0$	1.24(9)	-0.484(27)	1.273(46)	-0.469(15)	1.270(49)	-0.471(15)
$\Lambda_c^+ \rightarrow \Xi^0 K^+$	0.55(7)	0.01(16)	0.417(29)		0.545(69)	0.01(15)
$\Lambda_c^+ \rightarrow \Lambda^0 K^+$	0.0642(31)	-0.58(5)	0.0641(29)	-0.556(44)	0.0646(30)	-0.578(50)
$\Lambda_c^+ \rightarrow \Sigma^+\eta$	0.32(5)	-0.99(6)	0.327(49)	-0.9998(35)	0.328(49)	-0.978(57)
$\Lambda_c^+ \rightarrow \Sigma^+\eta'$	0.41(8)	-0.46(7)	0.416(65)	-0.455(64)	0.379(71)	-0.446(66)
$\Lambda_c^+ \rightarrow \Sigma^0 K^+$	0.0370(31)	-0.54(20)	0.0376(18)	-0.9971(36)	0.0363(27)	-0.47(17)
$\Lambda_c^+ \rightarrow n\pi^+$	0.066(13)		0.0641(23)		0.0646(91)	
$\Lambda_c^+ \rightarrow \Sigma^+ K_S^0$	0.047(14)		0.0311(29)		0.0341(88)	
$\Xi_c^+ \rightarrow \Xi^0\pi^+$	1.6(8)		0.880(78)		1.03(30)	
$\Xi_c^0 \rightarrow \Lambda K_S^0$	0.32(6)		0.248(29)		0.342(58)	
$\Xi_c^0 \rightarrow \Xi^-\pi^+$	1.43(27)	-0.640(51)	1.17(18)	-0.701(45)	1.25(19)	-0.643(51)
$\Xi_c^0 \rightarrow \Xi^- K^+$	0.039(11)		0.0520(80)		0.0488(75)	
$\Xi_c^0 \rightarrow \Sigma^0 K_S^0$	0.054(16)		0.056(16)		0.055(16)	
$\Xi_c^0 \rightarrow \Sigma^+ K^-$	0.18(4)		0.189(38)		0.185(40)	
$\Xi_c^0 \rightarrow \Xi^0\pi^0$	0.69(14)	-0.90(28)	0.153(48)	-0.45(13)	0.59(12)	-0.78(19)
$\Xi_c^0 \rightarrow \Xi^0\eta$	0.16(4)		0.166(37)		0.16(4)	
$\Xi_c^0 \rightarrow \Xi^0\eta'$	0.12(4)		0.125(38)		0.12(4)	

TABLE III: The predicted values for branching ratios, polarization parameters (α, β, γ) and CP violation with the final states $\eta^{(\prime)}$ for two different fits. Case I(II) means the fit results for the real(complex) form factors.

channel	Case I		Case II				
	Br(%)	α	Br(%)	α	β	γ	CPV
$\Lambda_c^+ \rightarrow \Sigma^+ \eta$	0.327(49)	-0.9998(35)	0.332(77)	-0.95(21)	-0.3(1.7)	0.1(2.2)	
$\Lambda_c^+ \rightarrow \Sigma^+ \eta'$	0.416(65)	-0.455(64)	0.409(99)	-0.409(88)	-0.70(59)	0.59(68)	
$\Lambda_c^+ \rightarrow p \eta$	0.154(10)	0.885(78)	0.162(21)	0.46(59)	-0.11(51)	-0.88(28)	-0.007(18)
$\Lambda_c^+ \rightarrow p \eta'$	0.0466(61)	-0.990(16)	0.056(15)	-0.90(34)	-0.43(68)	-0.04(49)	0.051(71)
$\Xi_c^+ \rightarrow \Sigma^+ \eta$	0.116(14)	0.91(11)	0.097(89)	0.50(45)	-0.04(1.71)	-0.87(24)	-0.020(57)
$\Xi_c^+ \rightarrow \Sigma^+ \eta'$	0.117(16)	-0.418(71)	0.125(56)	-0.31(24)	-0.84(60)	0.4(1.2)	0.037(53)
$\Xi_c^+ \rightarrow p \eta$	0.00908(67)	-0.054(61)	0.0105(41)	-0.12(13)	0.48(39)	-0.87(20)	
$\Xi_c^+ \rightarrow p \eta'$	0.0091(10)	-0.9957(86)	0.0100(63)	-0.82(44)	-0.58(59)	-0.01(1.10)	
$\Xi_c^0 \rightarrow \Xi^0 \eta$	0.177(75)	1.000(98)	0.107(99)	0.7(3.7)	-0.6(5.0)	-0.3(2.4)	
$\Xi_c^0 \rightarrow \Xi^0 \eta'$	0.121(83)	1.0(2.2)	0.10(21)	-0.7(2.9)	-0.2(16.8)	0.7(4.4)	
$\Xi_c^0 \rightarrow \Sigma^0 \eta$	0.020(14)	0.7(2.0)	0.020(42)	-0.1(3.2)	-0.9(1.9)	0.4(3.7)	-0.026(61)
$\Xi_c^0 \rightarrow \Sigma^0 \eta'$	0.0070(74)	1.0(2.6)	0.005(44)	-0.8(3.1)	-0.5(10.7)	0.4(11.5)	-0.04(28)
$\Xi_c^0 \rightarrow \Lambda \eta$	0.015(40)	0.9(2.6)	0.011(16)	-0.3(7.4)	-1.0(2.1)	-0.06(1.33)	-0.020(63)
$\Xi_c^0 \rightarrow \Lambda \eta'$	0.004(56)	0.4(23.2)	0.01(20)	0.6(2.6)	-0.3(9.3)	-0.8(5.0)	-0.002(189)
$\Xi_c^0 \rightarrow n \eta$	0.0008(34)	-0.2(1.7)	0.0017(33)	-0.2(1.8)	-0.5(1.4)	-0.82(73)	
$\Xi_c^0 \rightarrow n \eta'$	0.0005(52)	0.8(9.4)	0.0010(32)	-0.8(5.4)	-0.4(11.2)	-0.4(2.7)	

TABLE IV: The predicted values for branching ratios, polarization parameters (α, β, γ) and CP violation for two different fits. Case I(II) means the fit results for the real(complex) form factors.

channel	Case I		Case II				
	Br(%)	α	Br(%)	α	β	γ	CPV
$\Lambda_c^+ \rightarrow \Sigma^0 \pi^+$	1.259(46)	-0.471(15)	1.259(49)	-0.472(15)	0.75(13)	-0.46(20)	
$\Lambda_c^+ \rightarrow \Lambda \pi^+$	1.305(47)	-0.7538(60)	1.292(48)	-0.7551(60)	-0.480(75)	-0.446(81)	
$\Lambda_c^+ \rightarrow \Sigma^+ \pi^0$	1.273(46)	-0.469(15)	1.270(49)	-0.471(15)	0.75(13)	-0.47(20)	
$\Lambda_c^+ \rightarrow p K_S^0$	1.646(48)	0.41(12)	1.590(56)	0.05(27)	0.19(64)	-0.98(13)	
$\Lambda_c^+ \rightarrow \Xi^0 K^+$	0.417(29)	0.960(17)	0.545(69)	0.01(15)	-0.008(122)	0.9999(24)	
$\Xi_c^+ \rightarrow \Sigma^+ K_S^0$	0.79(21)	0.51(18)	0.60(76)	0.7(1.6)	-0.5(2.5)	0.48(58)	
$\Xi_c^+ \rightarrow \Xi^0 \pi^+$	0.880(78)	-0.892(39)	1.03(30)	-0.90(12)	0.43(24)	0.09(24)	
$\Xi_c^0 \rightarrow \Sigma^0 K_S^0$	0.056(16)	-0.55(26)	0.055(16)	-0.03(2.90)	0.07(2.74)	0.997(97)	
$\Xi_c^0 \rightarrow \Lambda K_S^0$	0.248(29)	0.87(15)	0.342(58)	-0.27(73)	-0.81(87)	-0.5(1.1)	
$\Xi_c^0 \rightarrow \Sigma^+ K^-$	0.189(38)	0.91(25)	0.185(40)	0.2(1.7)	-0.1(1.1)	-0.98(44)	
$\Xi_c^0 \rightarrow \Xi^- \pi^+$	1.17(18)	-0.701(45)	1.25(19)	-0.643(51)	0.06(1.39)	-0.76(12)	
$\Xi_c^0 \rightarrow \Xi^0 \pi^0$	0.153(48)	-0.45(13)	0.59(12)	-0.78(19)	-0.4(1.3)	-0.50(76)	
$\Lambda_c^+ \rightarrow \Sigma^0 K^+$	0.0376(18)	-0.9971(36)	0.0363(27)	-0.47(17)	-0.07(26)	-0.881(86)	0.003(23)
$\Lambda_c^+ \rightarrow \Lambda K^+$	0.0641(29)	-0.556(44)	0.0646(30)	-0.578(50)	0.810(41)	-0.10(20)	0.014(20)
$\Lambda_c^+ \rightarrow \Sigma^+ K_S^0/K_L^0$	0.0311(29)	-0.64(10)	0.0341(88)	-0.76(42)	0.59(97)	-0.28(99)	0.063(91)
$\Lambda_c^+ \rightarrow p \pi^0$	0.0174(53)	-0.10(13)	0.0160(71)	0.6(1.6)	-0.09(2.71)	0.79(95)	
$\Lambda_c^+ \rightarrow n \pi^+$	0.0641(23)	0.547(42)	0.0646(91)	-0.69(22)	-0.58(21)	0.43(15)	0.076(57)
$\Xi_c^+ \rightarrow \Sigma^0 \pi^+$	0.3175(88)	-0.731(17)	0.307(14)	-0.631(49)	0.578(97)	-0.52(14)	$0.0(1.1) \times 10^{-17}$
$\Xi_c^+ \rightarrow \Lambda \pi^+$	0.0211(32)	-0.19(18)	0.044(14)	0.55(32)	-0.69(38)	-0.48(29)	-0.10(11)
$\Xi_c^+ \rightarrow \Sigma^+ \pi^0$	0.273(18)	0.43(12)	0.261(62)	0.05(24)	0.40(32)	-0.92(13)	0.009(18)
$\Xi_c^+ \rightarrow p K_S^0/K_L^0$	0.164(15)	-0.451(82)	0.154(51)	-0.63(18)	0.49(97)	-0.60(68)	0.034(55)
$\Xi_c^+ \rightarrow \Xi^0 K^+$	0.1336(54)	0.382(33)	0.119(17)	-0.55(19)	-0.46(16)	0.696(92)	0.092(70)
$\Xi_c^0 \rightarrow \Sigma^0 \pi^0$	0.00002(12)	-0.99(74)	0.029(31)	-0.89(52)	-0.4(1.1)	-0.12(96)	-0.049(74)
$\Xi_c^0 \rightarrow \Lambda \pi^0$	0.0331(47)	0.74(11)	0.015(12)	-0.83(50)	0.3(1.1)	-0.44(55)	-0.035(43)
$\Xi_c^0 \rightarrow \Sigma^+ \pi^-$	0.0118(25)	0.89(27)	0.0120(26)	0.2(1.6)	-0.1(1.0)	-0.98(39)	
$\Xi_c^0 \rightarrow p K^-$	0.0146(39)	0.79(32)	0.0162(37)	0.1(1.3)	-0.10(83)	-0.99(25)	
$\Xi_c^0 \rightarrow \Sigma^- \pi^+$	0.0630(97)	-0.769(44)	0.083(13)	-0.577(49)	0.06(1.25)	-0.815(97)	$0.0(8.3) \times 10^{-18}$
$\Xi_c^0 \rightarrow n K_S^0/K_L^0$	0.0234(54)	0.40(25)	0.029(32)	0.18(49)	-0.54(81)	-0.82(58)	0.003(44)
$\Xi_c^0 \rightarrow \Xi^- K^+$	0.0520(80)	-0.656(44)	0.0488(75)	-0.687(52)	0.07(1.48)	-0.72(14)	$0.0(1.2) \times 10^{-17}$
$\Xi_c^0 \rightarrow \Xi^0 K_S^0/K_L^0$	0.0103(20)	0.59(33)	0.013(15)	0.25(62)	-0.74(85)	-0.6(1.1)	0.006(93)
$\Lambda_c^+ \rightarrow p K_L^0$	1.743(51)	0.48(12)	1.685(60)	0.11(30)	0.15(66)	-0.98(12)	
$\Lambda_c^+ \rightarrow n K^+$	0.001009(90)	-0.975(21)	0.00130(37)	-0.89(12)	0.43(24)	-0.17(23)	
$\Xi_c^+ \rightarrow \Sigma^0 K^+$	0.01142(30)	-0.9964(13)	0.01104(52)	-0.699(58)	-0.07(13)	-0.712(52)	
$\Xi_c^+ \rightarrow \Lambda K^+$	0.00441(18)	0.615(30)	0.00374(52)	-0.34(19)	0.892(75)	0.30(28)	
$\Xi_c^+ \rightarrow \Sigma^+ K_L^0$	0.98(23)	0.74(15)	0.77(85)	0.8(1.3)	-0.5(2.2)	0.17(67)	
$\Xi_c^+ \rightarrow p \pi^0$	0.00067(25)	0.06(32)	0.0008(15)	0.4(1.6)	0.7(1.2)	-0.6(2.2)	
$\Xi_c^+ \rightarrow n \pi^+$	0.00607(39)	0.939(21)	0.00407(51)	0.02(29)	-0.01(23)	0.9997(88)	
$\Xi_c^0 \rightarrow \Sigma^0 K_L^0$	0.070(18)	-0.27(28)	0.074(47)	-0.3(2.3)	-0.1(2.7)	0.95(98)	
$\Xi_c^0 \rightarrow \Lambda K_L^0$	0.230(26)	0.91(12)	0.321(71)	-0.32(75)	-0.82(86)	-0.5(1.1)	
$\Xi_c^0 \rightarrow p \pi^-$	0.00087(24)	0.77(33)	0.00098(23)	0.1(1.3)	-0.09(79)	-0.99(23)	
$\Xi_c^0 \rightarrow \Sigma^- K^+$	0.00285(44)	-0.736(45)	0.00338(51)	-0.609(50)	0.06(1.32)	-0.79(11)	
$\Xi_c^0 \rightarrow n \pi^0$	0.00162(25)	0.993(32)	0.00045(29)	-0.7(1.1)	0.50(45)	0.5(1.9)	